Laser ablation of a metal foam: role of electron-phonon coupling and electronic heat diffusivity

Yudi Rosandi,[1] Joás Grossi,[2] Eduardo M. Bringa,[2] and Herbert M. Urbassek[3,*]

[1] *Department of Physics, Universitas Padjadjaran, Jatinangor, Sumedang 45363, Indonesia*
[2] *CONICET and Facultad de Ciencias Exactas y Naturales, Universidad Nacional de Cuyo, M5502JMA Mendoza, Argentina*
[3] *Fachbereich Physik und Forschungszentrum OPTIMAS, Universität Kaiserslautern, Erwin-Schrödinger-Straße, D-67663 Kaiserslautern, Germany*

(Dated: December 4, 2017)

Incidence of energetic laser pulses on a metal foam may lead to foam ablation. The processes occurring in the foam may differ strongly from those in a bulk metal: The absorption of laser light, energy transfer to the atomic system, heat conduction, and finally the atomistic processes – such as melting or evaporation – may be different. In addition, novel phenomena take place, such as a reorganization of the ligament network in the foam. We study these processes for the example of a Au foam of average porosity 79 % and average ligament diameter of 2.5 nm, using molecular dynamics simulation. The coupling of the electronic system to the atomic system is modeled by using the electron-phonon coupling, g, and the electronic heat diffusivity, κ_e, as model parameters, since their actual values for foams are unknown. We show that the foam coarsens under laser irradiation. While κ_e governs the homogeneity of the processes, g mainly determines their time scale. The final porosity reached is independent of the value of g.

Keywords: Laser materials processing, laser irradiation, molecular dynamics, Au, ablation

I. INTRODUCTION

The theoretical understanding of laser ablation by ultrafast pulses has reached a mature level of understanding [1–3]. This applies both to metallic and insulating surfaces; however, the situation in metals is particularly transparent. Visible or ultraviolet laser light is absorbed by the conduction electrons, which can transport the energy further away from the surface by diffusion; by electron-phonon coupling the energy is conveyed to the atomic system. Melting, evaporation and ablation processes can then occur in the atomic system.

Molecular dynamics (MD) simulations have demonstrated a high capability of modeling the materials processes occurring in a metal after irradiation, since thermal heating, the action of tensile and compressive pressures, and phase transformations (melting, evaporation) are automatically included in the description of the material as soon as an appropriate interatomic interaction force has been included [4]. The dynamics of the electron system and its coupling to the atoms is treated with the so-called two-temperature model (TTM), which describes the electron dynamics with the help of a heat diffusion equation [4, 5].

Surface nanostructuring induced by laser ablation has been investigated [6], but up to now mostly flat metal surfaces have been investigated and the modeling of laser irradiation on nanostructured surfaces has been limited [7]. An extreme case of such nanostructures is provided by metallic nanofoams. Their geometry is characterized by their porosity, which describes the global fraction of space occupied by atoms, and by the ligament diameter, which characterizes the nanoscale of the material.

The mechanical behavior of foam material may differ strongly from that of a bulk metal [8]; but several experimental results can be explained by MD simulations [9, 10]. However, the behavior of the excited electronic system in the irradiated foam poses several interesting problems. Ballistic and diffusive motion of the electrons (heat conduction) is hampered by the foamy structure, both due to geometric constraints (transport occurs only in the ligaments) and due to an increase of scattering processes at the ligament walls. Theoretical assessments for the dependence of the ligament diameter on the heat diffusivity are available [11], but not for the entire foamy structure. A second issue is related to the electron-phonon coupling; since both electron and phonon density of states change in the ligaments and in the entire foam structure [12], electron-phonon coupling is expected to change as well [13]. However, here, to our knowledge, no theoretical prediction could be obtained.

In the present study, we explore the heating of a metallic foam by an ultrashort laser pulse using MD simulation for the example of a Au foam. In view of the uncertainties of the parameters describing the electron system and its coupling to the atoms, we treat the electron-phonon-coupling, Sect. III A, and the electronic heat diffusivity, Sect. III C, as model parameters, which we change freely in order to observe their effects on the ablation behavior. Results on structural changes will be discussed in Sect. III B.

*Electronic address: urbassek@rhrk.uni-kl.de; URL: http://www.physik.uni-kl.de/urbassek/

II. METHOD

Foam construction starts from the observation that at any given time, local temperatures in a liquid will not coincide with the global (average) temperature; we use the isotherms to define non-simply connected structures that can be used as a model for a foam structure. Further details of the method are outlined in [14]. This method allows us to construct films of predefined porosity with values between 25% and 85%. The foam used in the present study has a porosity of $p = 79$ %. The average ligament size is around 2.5 nm.

Fig. 1 shows the structure of the nanofoam we use. It has a thickness of 130 nm and a square cross section of side length 13 nm. Periodic boundary conditions are applied at the lateral sides, while the top and bottom surfaces are left free. Au atoms fill up the foam such that the ligaments have a single-crystalline structure with top and bottom surfaces aligned along the (100) crystal axis. We relax the samples to a temperature of 300 K and the average pressure 0.

The TTM solves the continuum equation for the electronic system coupled to an MD simulation of the atomic system. The MD simulation is performed using LAMMPS [15] with a time step of $\Delta t = 1$ fs. **This time step is sufficiently small to allow for a stable integration of Newton's equation of motion [4].**The interaction between Au atoms is described by the embedded-atom-method potential as proposed by Foiles *et al.* [16] using a cut-off distance of $r_c = 4.94$ Å. **This potential satisfactorily describes elastic and thermal properties of Au such as elastic constants, surface energies and sublimation energy.**

The space and time dependence of the electron temperature, T_e, is described by the heat diffusion equation,

$$C_e \frac{\partial T_e}{\partial t} = \nabla \left(\kappa_e \nabla T_e\right) - g\left[T_e - T_a\right] + \Phi\,. \tag{1}$$

Here C_e, κ_e and g are the electronic heat capacity, heat conductivity, and electron-phonon coupling, respectively. All of these quantities are functions of the electronic temperature. C_e and g are provided in Ref. 17, while $\kappa = \kappa_0 T_e/T_a$ with $\kappa_0 = 0.1998$ eV/(psKÅ) [18]. The atom temperature $T_a(\mathbf{r}, t)$ is calculated from the MD simulation as a local average over a sphere with a radius taken as the cut-off radius of the potential [19, 20].

We assume the laser pulse to have a Gaussian time distribution with maximum at time $t_0 = 1$ ps and width $\sigma = 0.2$ ps:

$$f(t) = \frac{1}{\sqrt{2\pi}\sigma} \exp\left[-\frac{1}{2}\left(\frac{t - t_0}{\sigma}\right)^2\right]. \tag{2}$$

The source term $\Phi(\mathbf{r}, t)$ in Eq. (1) is given by

$$\Phi(\mathbf{r}, t) = E_0 n_0 f(t) e^{-\zeta/\lambda}, \tag{3}$$

where $n_0 = 0.0589$ Å^{-3} is the equilibrium target atom number density. E_0 is the energy that a surface atom receives from the laser pulse; we use here the value $E_0 = 5$ eV/atom; the surface energy density is $\epsilon_0 = E_0 n_0 = 0.295$ eV/Å^3.

For a bulk material, the coordinate ζ would simply measure the depth below the surface; for our case of a strongly inhomogeneous foam, ζ measures the thickness of solid material between the point, where $\Phi(\mathbf{r}, t)$ is evaluated and the surface. This recipe assumes that no laser energy is absorbed in the voids, but only in the ligaments of the foam. The absorption length λ assumes the value 168 Å [21].

Eq. (1) is solved using a three-dimensional finite-difference scheme with a cell size of $\Delta x = 4.08$ Å, corresponding to the lattice constant of Au, and a time step of the order of 10^{-17} s [5]. The number of atoms in each cell is monitored; if the atom density decreases below 1/6 of the solid density, n_0, the electronic heat diffusivity is set to zero in this cell [7].

We apply the velocity-scaling method to exchange energy between the atomic and electronic system [22]. The amount of energy density put into the atomic system every time step is $\Delta\epsilon = g[T_e - T_a]\Delta t$, where Δt is the time step of the MD simulation. Energy is only put into thermal atomic motion, using the recipe provided in Ref. 22.

The simulation is run until 200 ps after irradiation.

The two main parameters characterizing the electronic system and its coupling to the atomic system are the electron-phonon coupling constant g and the electron heat diffusivity, κ_e. While the values in bulk Au are well known [17], the values in nanomaterials such as a Au foam may differ strongly from these and are not well known. We therefore use scaling factors $G = 0.1$, 1, 10 to model the electron-phonon coupling constant

$$g_{\text{sim}} = Gg \tag{4}$$

and $k = 0.1$, 1 to model the electron heat diffusivity,

$$\kappa_{\text{sim}} = k\kappa_e. \tag{5}$$

Note that only smaller electron heat diffusivities than the bulk values are considered since small ligaments will have reduced diffusivities.

The rendering of structures is performed with OVITO [23].

III. RESULTS

A. Influence of electron-phonon coupling

First we explore the effect of the electron-phonon coupling g on the evolution of the irradiated foam. Fig. 2a shows how quickly electronic and atomic temperatures equilibrate; the data show temperature averages over the entire film. The electron temperature increases until the end of the laser pulse and then decreases as energy is transferred to the atom system. Atom temperature monotonically increases; the final temperatures

amount to around 4000 K in all cases. However, the time when equilibrium is reached, $t_{\rm equ}$, depends strongly on the electron-phonon coupling. For the standard value, $G = 1$, it is $t_{\rm equ} = 40$ ps, while this value decreases to $t_{\rm equ} = 4$ ps for the tenfold increased electron-phonon coupling. For the smallest value of g used, no equilibrium is established until the end of our simulation (200 ps). Thus a dependence $t_{\rm equ} \propto g^{-1}$ may be read off these data. These numbers are in agreement with a simple estimate of electron-phonon equilibration in laser-irradiated metals; assuming a homogeneous energization with energy density ϵ_0, these predict [4]

$$t_{\rm equ} = \sqrt{2\gamma\epsilon_0}/g. \qquad (6)$$

Here γ is the prefactor of the electronic specific heat in the linear approximation, $C_e = \gamma T_e$, which amounts to 67.6 J/m^3 K^2 for Au [17]. For the standard value of $g = 3 \times 10^{16}$ W /m^3 K [17], Eq. (6) predicts $t_{\rm equ} = 84$ ps, which is of the same order but a factor of 2 above our simulation results. The deviation is due to a combination of several effects: (i) g increases with temperature; (ii) the energy density ϵ_0 decreases with depth; both factors lower $t_{\rm equ}$.

The spatial profiles, taken at a time of 5 ps, are shown in Fig. 2b. They demonstrate a qualitatively similar distribution; this is plausible since the spatial dependence is mainly governed by the electron heat diffusivity, which is identical in all cases. However, the temperature contrast between front and back side is smaller for the cases of small g.

This is caused by a self-amplifying process: since g is an increasing function of atom temperature, as soon as high temperatures are reached, electrons couple even more effectively to phonons and the heating rate increases. For low g, also energy transfer to phonons is slower, and hence electronic heat diffusion has more time to homogenize the profile.

Fig. 3 shows snapshots of the foams at 5 and 100 ps after irradiation. Let us first discuss the results at 5 ps. The foam with the lowest electron-phonon coupling shows a rather homogeneous state of the material at 5 ps. Density contrasts are strong, evaporation has not yet started, and also the film coarsening induced by melting is not yet pronounced. On the other extreme, the $G = 10$ foam shows strong inhomogeneities in its evolution; evaporation on the front side is already pronounced, while it is absent on the rear side. Foam fragmentation and dissolution has already started on the front side; there the density difference between remaining condensed material and the gas phase is strongly decreased. Here it is also evident that the melting transition does not contribute to the process, as the temperatures are so high that the material immediately is heated above the critical point of the liquid-gas phase transition – 7400 K [24] – and becomes supercritical. The evolution for the standard case, $G = 1$, is intermediate between these two cases.

At 100 ps, evaporation has also started in the $G = 0.1$ foam. The condition of the metal in the surface-near part has now become indistinguishable from the standard case, $G = 1$, and the case of high electron-phonon-coupling, $G = 10$; a mixture of large clusters of low density and gas has developed. This situation is typical for high-fluence ablation [25]. At the rear side, evaporation from both foams has started, while the pore structure is still clearly discernible.

An evaluation of the pressure (not shown) demonstrates strong compressive thermoelastic pressures in the first 5 ps after irradiation, reaching values of up to 1 GPa. In particular for the largest value of the electron-phonon-coupling, we also observe tensile pressures developing in the near-surface region; these are caused by the rapid expansion and are related to the dissolution of the structure to a mixture of gas and large clusters. However, already at 6 ps the pressures have relaxed to values of the order of 100 MPa and fluctuate strongly in the specimens.

We conclude that the value of the electron-phonon coupling governs the time dependence of the materials effects; to a lesser degree it also influences the energy homogenization in the sample, since in Au, g increases with temperature.

B. Porosity

After irradiation, the film structure changes; we quantify it using the concept of porosity. In order to define porosity, a distinction has to be made between the condensed phase (solid or liquid) and the vacuum or gas phase. We use the criterion that the gaseous phase is defined by an atom number density below $n = 0.024$ Å^{-3}; this value was determined from inspection of the density plots. Porosity, p, is defined as

$$p = 1 - \frac{V_{\rm cond}}{V}, \qquad (7)$$

where V is the volume of the specimen, and $V_{\rm cond}$ is the part of the volume filled by condensed matter. The determination of $V_{\rm cond}$ requires to trace out the surface of irregularly shaped volumes; this is accomplished with the help of the so-called alpha-shape method [26, 27] implemented within the Crystal Analysis Tool (CAT) [28–30]. The identification of the surface requires the use of a 'probe sphere' rolling over it; its radius has been set to the values of 0.4 and 0.5 nm, somewhat larger than the nearest-neighbor distance in Au. The difference between the resulting porosities for the two radii is used to define error bars in our determination of p.

Fig. 4 displays the time evolution of the porosity in the film for the three electron-phonon couplings investigated. In all three cases, film coarsening is observed, that is a reduction in porosity. This feature is already visible in the snapshots, Fig. 3; it is caused by the action of surface tension in the molten phase which compactifies the ligament structures, and tends to close small void structures.

In all three cases, the porosity finally reached assumes similar values (within the error bars) of around 0.7.

Porosity changes monotonically for the smallest value of the electron-phonon coupling, $G = 0.1$. In the other cases observed, voids are quickly filled by evaporated gas atoms and clusters; this tends to complicate the porosity analysis. In particular, in the early phase after irradiation – up to 50 ps after irradiation – the analysis is dominated by fluctuations. However, at later times, all curves show the same trend featuring a decreasing porosity which leads to the same final saturation value.

We also tried to measure void sizes in the irradiated film. However, due to the irregular structures of the voids, no clear trend in the evolution of void sizes could be determined.

We conclude that porosity decreases due to film melting; the value of the electron-phonon-coupling induces different transient behaviors connected to the time scale of phase changes (melting and evaporation).

C. Influence of electronic heat diffusivity

Up to now we used the standard value of the electron heat diffusivity, $k = 1$, Eq. (5), which applies to bulk Au samples. However, the electron heat diffusivity in thin ligaments is expected to be smaller than in bulk samples [11]; we explore the effect of a decreased diffusivity with a simulation for a tenfold smaller value, $k = 0.1$, but for the standard value of the electron-phonon coupling.

Fig. 5 demonstrates the influence of the heat diffusivity on the spatial profile of the atom temperature in the irradiated slab at times of 5 and 100 ps after irradiation. The larger electron diffusivity leads to a more efficient homogenization of the temperature in the film; this is apparent at both times studied. Since the laser absorption length is only 168 Å, at the early time, electron diffusion could not yet homogenize the temperature even for the higher (bulk) value of the diffusivity, temperatures have equilibrated for $k = 1$ at 100 ps. For $k = 0.1$, at this time the backside of the film is still considerably cooler (around 3000 K) than the front side (around 5500 K).

Fig. 6 compares the film structures at a time of 100 ps after irradiation. Strong changes in the film structure are visible in the front side. Due to the higher temperatures still present there for the smaller heat diffusivity, the foam structure has strongly dissolved to a gas cloud consisting of atoms and larger clusters; this picture of material fragmentation is reminiscent of spinodal decomposition occurring when matter is brought in the vicinity of the critical temperature of the liquid-gas phase transition and has been observed previously in the atomistic simulation of laser irradiation (bulk) metals [4, 25, 31].

In contrast, the higher temperatures in the rear part of the foam for $k = 1$ lead to more massive evaporation from the back side.

The influence of the lowered value of the heat conduction on the porosity is included in Fig. 4. The initial behavior parallels that of the standard case, $G = 1$, $k = 1$; however, the porosity values stay high and do not decrease below $p \sim 0.74$. This decreased coarsening is in agreement with the inhomogeneous temperature profile for low heat conductivities, Fig. 5, which leaves the back part of the film unchanged while the front part suffers strong evaporation, see the snapshots of Fig. 6.

IV. SUMMARY

Laser irradiation of metallic foams is still poorly understood, since the behavior of the electronic system after irradiation may deviate from that of a bulk metal. Thus, the heat diffusivity of electrons is assumed to be smaller than in the bulk, due to restrictions of electronic motion in the ligaments. Also the electron-phonon coupling may be changed; here, however, it is not clear whether it is enhanced or decreased with respect to bulk values. We therefore performed simulations within the framework of the TTM to explore the influence of these two parameters on ablation from laser irradiated foams.

Our results demonstrate that the magnitude of the electron-phonon coupling is decisive for the time scale within which energy is transferred to the atomic system, and hence the speed of melting and evaporation processes. To a lesser degree it also influences the energy homogenization in the sample, since in Au, it increases with temperature. Heat conduction, on the other hand, mainly determines the homogeneity of the energy profile in the specimen. While a low heat diffusivity may localize the irradiated energy near the front surface and increase ablation there, a high value may transport energy quickly to the back side and enhance the processes there.

The final porosity reached is independent of the value of the electron-phonon coupling; it depends, however, on the heat conduction in that low heat conductivities lead to smaller changes of the porosity.

The modeling of ablation processes in foams within the TTM is hampered in particular by the difficulties of solving the electron heat conduction equation in three dimensions in a strongly inhomogeneous system. Future work will concentrate on identifying the influence of porosity and ligament thickness on the ablation behavior, explore the dependence of the processes on the absorbed laser energy, and attempt to extend the simulations to other metals.

Metallic nanofoams display heat conductivities that are only a few times smaller than for bulk samples. However, semiconductor and oxide nanofoams may have thermal conductivities that are more than one order of magnitude lower than in the bulk [32]. TTM models have to be modified to be applicable to semiconductors [33], but large changes in ablation may be expected.

Acknowledgments

We appreciate the computational resources provided by the computer cluster 'Elwetritsch' of the University of Kaiserslautern. YR is grateful for funding from the Indonesian Directorate General of Higher Education (DIKTI), contract No. 718/UN6.3.1/PL/2017. JG and EMB acknowledge support from SeCTyP-UNCuyo Grant No. M003, from ANPCyT Grant No. PICT-2014-0696, and from CONICET.

[1] C. Wu and L. V. Zhigilei, Appl. Phys. A **114**, 11 (2014).
[2] M. V. Shugaev, C. Wu, O. Armbruster, A. Naghilou, N. Brouwer, D. S. Ivanov, T. J.-Y. Derrien, N. M. Bulgakova, W. Kautek, B. Rethfeld, et al., MRS Bull. **41**, 960 (2016).
[3] B. Rethfeld, D. S. Ivanov, M. E. Garcia, and S. I. Anisimov, J. Phys. D **50**, 193001 (2017).
[4] H. M. Urbassek, in *Handbook of surface science*, edited by E. Hasselbrink and B. I. Lundqvist (Elsevier, Amsterdam, 2008), vol. 3. Dynamics, chap. 17, pp. 871–913.
[5] C. Schäfer, H. M. Urbassek, and L. V. Zhigilei, Phys. Rev. B **66**, 115404 (2002).
[6] C. Wu and L. V. Zhigilei, The Journal of Physical Chemistry C **120**, 4438 (2016).
[7] Y. Rosandi and H. M. Urbassek, Appl. Surf. Sci. **307**, 142 (2014).
[8] J. Biener, A. M. Hodge, J. R. Hayes, C. A. Volkert, L. A. Zepeda-Ruiz, A. V. Hamza, and F. F. Abraham, Nano Lett. **6**, 2379 (2006).
[9] C. J. Ruestes, D. Farkas, A. Caro, and E. M. Bringa, Acta Materialia **108**, 1 (2016), ISSN 1359-6454.
[10] B.-N. D. Ngo, A. Stukowski, N. Mameka, J. Markmann, K. Albe, and J. Weissmüller, Acta Mater. **93**, 144 (2015).
[11] P. E. Hopkins, P. M. Norris, L. M. Phinney, S. A. Policastro, and R. G. Kelly, J. Nanomater. **2008**, 418050 (2008).
[12] P. E. Hopkins, P. T. Rakich, R. H. Olsson, I. F. El-kady, and L. M. Phinney, Appl. Phys. Lett. **95**, 161902 (2009).
[13] J. L. Hostetler, A. N. Smith, D. M. Czajkowsky, and P. M. Norris, Appl. Optics **38**, 3614 (1999).
[14] N. Gunkelmann, Y. Rosandi, C. J. Ruestes, E. M. Bringa, and H. M. Urbassek, Comput. Mater. Sci. **119**, 27 (2016).
[15] S. Plimpton, J. Comput. Phys. **117**, 1 (1995), *http://lammps.sandia.gov/*.
[16] S. M. Foiles, M. I. Baskes, and M. S. Daw, Phys. Rev. B **33**, 7983 (1986).
[17] Z. Lin, L. V. Zhigilei, and V. Celli, Phys. Rev. B **77**, 075133 (2008), http://www.faculty.virginia.edu/CompMat/electron-phonon-coupling/.
[18] J. Hohlfeld, S.-S. Wellershoff, J. Güdde, U. Conrad, V. Jähnke, and E. Matthias, Chem. Phys. **251**, 237 (2000).
[19] T. J. Colla and H. M. Urbassek, Radiat. Eff. Defects Solids **142**, 439 (1997).
[20] A. K. Upadhyay and H. M. Urbassek, J. Phys. D **40**, 3518 (2007).
[21] D. Bäuerle, *Laser processing and chemistry* (Springer, Berlin, 2000), 3rd ed.
[22] Y. Rosandi and H. M. Urbassek, Appl. Phys. A **110**, 649 (2013).
[23] A. Stukowski, Model. Simul. Mater. Sci. Eng. **18**, 015012 (2010), *http://www.ovito.org/*.
[24] K. Boboridis, G. Pottlacher, and H. Jäger, Int. J. Thermophys. **20**, 1289 (1999).
[25] A. K. Upadhyay, N. A. Inogamov, B. Rethfeld, and H. M. Urbassek, Phys. Rev. B **78**, 045437 (2008).
[26] H. Edelsbrunner and E. P. Mücke, ACM Trans. Graphics **13**, 43 (1994).
[27] A. Stukowski, JOM **66**, 399 (2014).
[28] A. Stukowski, V. V. Bulatov, and A. Arsenlis, Model. Simul. Mater. Sci. Eng. **20**, 085007 (2012).
[29] A. Stukowski, Model. Simul. Mater. Sci. Eng. **20**, 045021 (2012).
[30] A. Stukowski and A. Arsenlis, Model. Simul. Mater. Sci. Eng. **20**, 035012 (2012).
[31] L. V. Zhigilei, Z. Lin, and D. S. Ivanov, J. Phys. Chem. C **113**, 11892 (2009).
[32] Y. He, D. Donadio, J.-H. Lee, J. C. Grossman, , and G. Galli, ACSNano **5**, 1839 (2011).
[33] G. S. Khara, S. T. Murphy, S. L. Daraszewicz, and D. M. Duffy, Journal of Physics: Condensed Matter **28**, 395201 (2016).

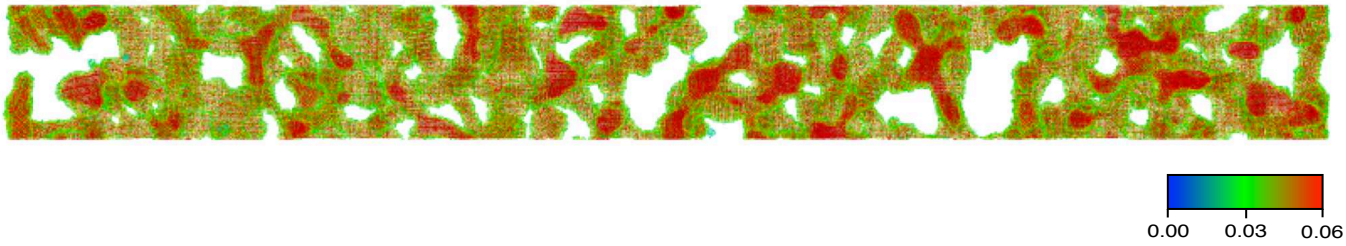

FIG. 1: Snapshot showing the foam structure immediately before irradiation. **Color codes density (in units of Å^{-3}), see color bar.** Top surface is at the right and rear surface at the left. The structure is repeated periodically in the lateral directions.

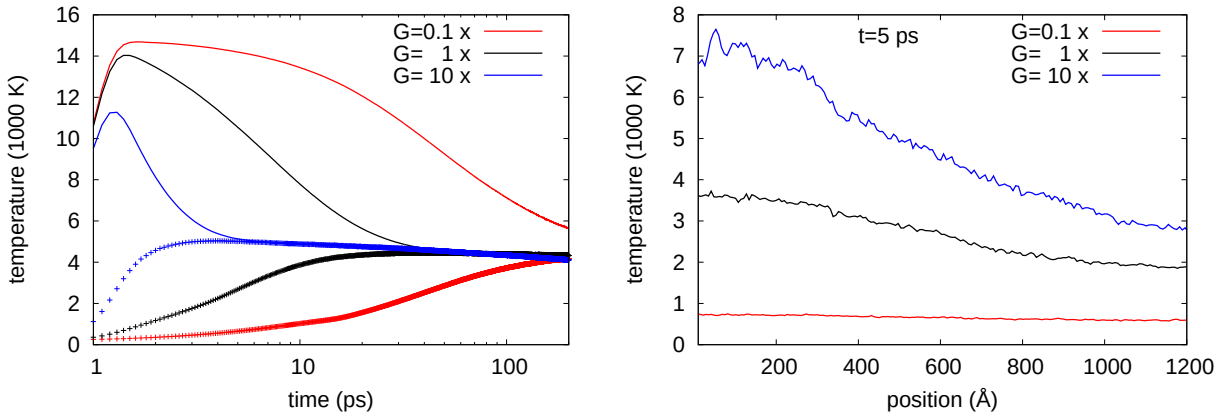

FIG. 2: Electron and atom temperatures in the foam for three values of the electron-phonon coupling constant G. (a) Time evolution of spatially averaged temperatures. Line: electronic system; symbols: atomic system. (b) Space dependence of the atomic temperature at time $t = 5$ ps.

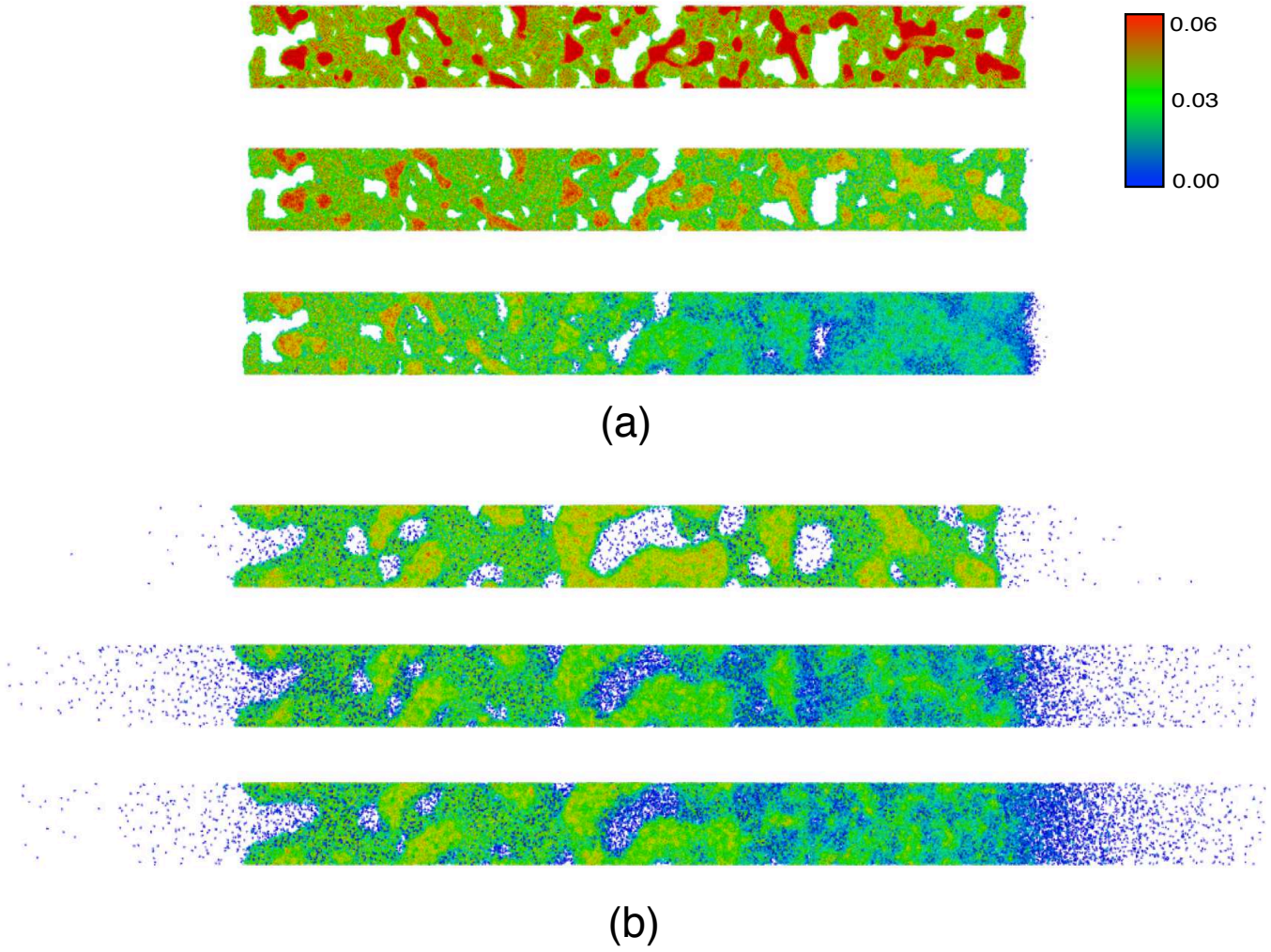

FIG. 3: Snapshots of the foam at time (a) $t = 5$ ps and (b) $t = 100$ ps for $G = 0.1$ (top), $G = 1$ (middle), and $G = 10$ (bottom). Color codes density (in units of Å^{-3}), see color bar. The laser irradiates from the left side.

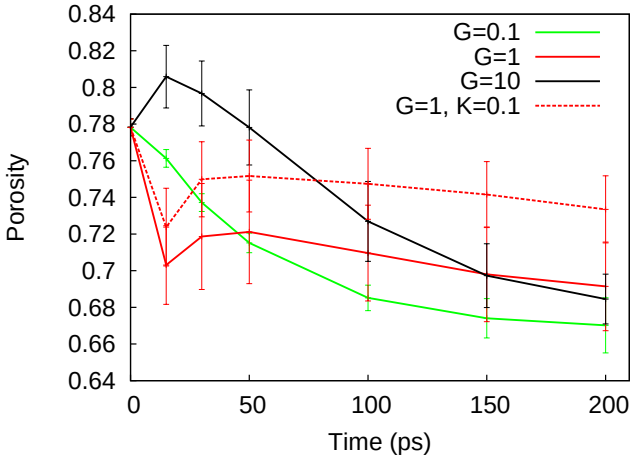

FIG. 4: Temporal evolution of porosity in the foam.

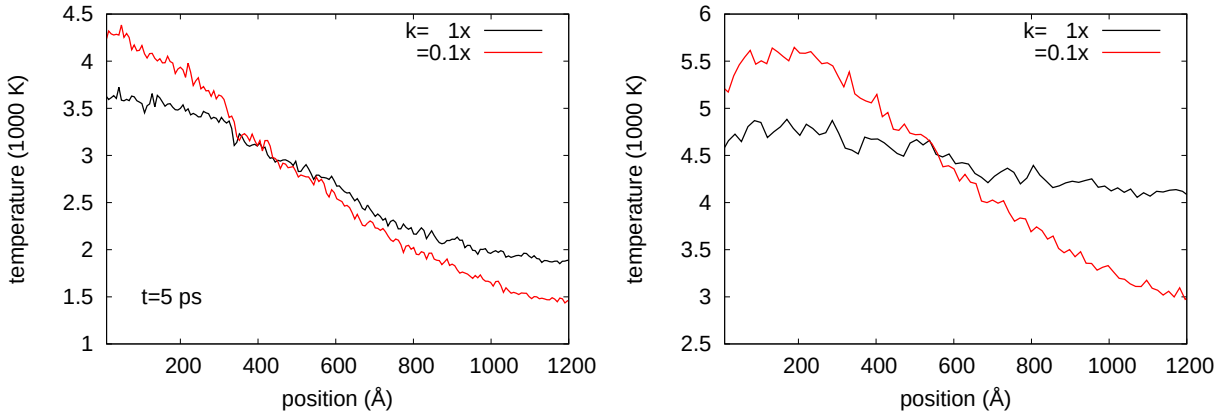

FIG. 5: Space dependence of the temperature at time (a) $t = 5$ ps, (b) 100 ps. Data are for a simulation with standard electronic heat diffusivity, $k = 1$, and with a reduced diffusivity, $k = 0.1$. Standard electron-phonon coupling, $G = 1$, was assumed in both cases.

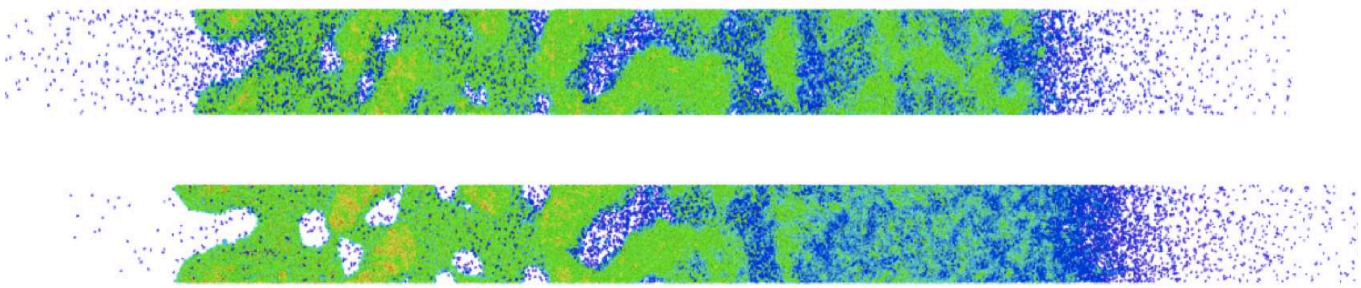

FIG. 6: Snapshot of the irradiated foam (reduced electronic heat diffusivity) at time $t = 100$ ps. Top: standard electronic heat diffusivity, $k = 1$. Bottom: reduced diffusivity, $k = 0.1$. Standard electron-phonon coupling, $G = 1$, was assumed in both cases.